Article:
Lehman, JH orcid.org/0000-0001-6610-6519 and Lester, MI (2014) Dynamical Outcomes of Quenching: Reflections on a Conical Intersection. Annual Review of Physical Chemistry, 65 (1). pp. 537-555. ISSN 0066-426X

https://doi.org/10.1146/annurev-physchem-040513-103628

Dynamical Outcomes of Quenching:

Reflections on a Conical Intersection

Julia H. Lehman and Marsha I. Lester*
Department of Chemistry, University of Pennsylvania,
Philadelphia, PA 19104-6323 USA

Abstract

This review focuses on experimental studies of the dynamical outcomes following collisional quenching of electronically excited OH $A\ ^2\Sigma^+$ radicals by molecular partners. The experimental observables include the branching between reactive and nonreactive decay channels, kinetic energy release, and quantum state distributions of the products. Complementary theoretical investigations reveal regions of strong nonadiabatic coupling, known as conical intersections, which facilitate the quenching process. The dynamical outcomes observed experimentally are connected to the local forces and geometric properties of the nuclei in the conical intersection region. Dynamical calculations for the benchmark OH-H_2 system are in good accord with experimental observations, demonstrating that the outcomes reflect the strong coupling in the conical intersection region as the system evolves from the excited electronic state to quenched products.

* Corresponding author email: milester@sas.upenn.edu

I. Introduction

The hydroxyl radical is an important species in atmospheric and combustion environments,(1, 2) where it is often detected by laser-induced fluorescence (LIF) on the well-characterized $A\ ^2\Sigma^+ - X\ ^2\Pi$ band system.(3) Although electronic excitation of isolated OH radicals on the *A*-*X* transition would simply result in radiative decay, collisions of electronically excited OH $A\ ^2\Sigma^+$ with partners prevalent in these environments open up alternative nonradiative decay pathways that efficiently remove OH from the excited electronic state. As a result, the OH $A \rightarrow X$ fluorescence emission is partially or fully quenched. At a practical level, the rates for collisional quenching of OH $A\ ^2\Sigma^+$ by relevant species must be taken into account in order to utilize LIF for quantitative measurements of OH concentrations under these conditions.(4, 5) At a more detailed level, one would like to know the mechanism for collisional quenching of OH $A\ ^2\Sigma^+$ by at least a few simple partners. Specifically, does collisional quenching occur via reactive and/or nonreactive processes? What is the branching between these processes? Can additional insights on the mechanism be inferred from the partitioning of the initial electronic energy over internal and translational degrees of freedom in the quenched products? At a fundamental level, one would like to understand the nature of the coupling between the OH $A\ ^2\Sigma^+$ and $X\ ^2\Pi$ electronic states in the presence of the collision partner that gives rise to quenching. The nonadiabatic coupling between electronic states involves a breakdown of the Born-Oppenheimer approximation and the intrinsic assumption that nuclear motion evolves on a single adiabatic electronic potential energy surface.(6) Such nonadiabatic processes occur in the photophysics of many molecular systems, ranging from ethylene to DNA, in both gaseous and condensed phases, and are an active area of experimental and theoretical research in chemical physics today.(7-11)

The collisional quenching of OH $A\ ^2\Sigma^+$ by simple molecular partners, e.g. H_2, N_2, CO, CO_2, O_2, and Kr, provide a rich test bed in which to explore the underlying mechanism for quenching. In recent years, it has become possible to extend the kinetic rate studies to dynamical measurements that examine the outcomes of quenching, including branching between reactive and nonreactive decay processes, kinetic energy release, and quantum state distributions of the products.(12-24) The experimental results exhibit similarities in the outcomes of OH $A\ ^2\Sigma^+$

quenching with several collision partners, suggesting common features about the nonadiabatic dynamics. For a few of the OH $A\ ^2\Sigma^+$ + M systems studied experimentally, specifically M= H_2, N_2, CO, and Kr, theoretical investigations have identified regions of strong nonadiabatic coupling, known as conical intersections (CI), that facilitate the quenching process.(16, 18-20, 25, 26)

The four-atom OH $A\ ^2\Sigma^+$ + H_2 system has emerged as a model system for examining the nonadiabatic coupling and associated dynamics for collisional quenching. For this system, experimental studies have been complemented by first-principles theoretical calculations of the CI regions that couple the OH ($A\ ^2\Sigma^+$, $X\ ^2\Pi$) + H_2 potentials, including the reactive channel to H + H_2O products, as well as dynamical calculations of the outcomes.(16, 17, 25-31) Figure 1 illustrates the minimum energy path from the OH $A\ ^2\Sigma^+$ + H_2 asymptote with the O-side of OH pointing toward H_2 to a CI in the HO-H_2 configuration.(25) Two pathways then emerge from the intersection, leading to OH $X\ ^2\Pi$ + H_2 products (nonreactive quenching) and H + H_2O products (reactive quenching). This one-dimensional picture highlights key features of OH quenching by several partners: restricted access from the OH $A\ ^2\Sigma^+$ + M asymptote to the downhill path leading to the CI region, branching in the CI region to multiple product channels, and evolution to OH $X\ ^2\Pi$ + M and other reaction products.

This review focuses on experimental studies of outcomes following collisional quenching of OH $A\ ^2\Sigma^+$ and related theoretical investigations of the nonadiabatic couplings and dynamics. As will be discussed, the experimental observables provide a reflection of the forces on the nuclei as the system evolves from the excited electronic state through regions of strong nonadiabatic coupling to separated quenched products. The quenching outcomes contain signatures of the nonadiabatic dynamics, and thereby enable new insights on the mechanism for collisional quenching of OH $A\ ^2\Sigma^+$ by simple molecular partners.

II. Quenching Kinetic Studies

Prior kinetic studies have evaluated the bimolecular rate constants k_Q and corresponding cross sections σ_Q for electronic quenching of OH $A\ ^2\Sigma^+$ by various collision partners of importance in atmospheric and combustion environments, e.g. N_2, O_2, CO, CO_2, H_2O.(5, 32-35) LIF studies of OH radicals on the *A-X* transition in these environments are

subject to significant quenching of the induced fluorescence from the excited $A\ ^2\Sigma^+$ state. This is evident from reduced fluorescence quantum yields Φ and shortened fluorescence lifetimes τ at atmospheric pressure.(36-38)

The rate coefficients for quenching have been examined over the temperature ranges relevant in these environments and as a function of the OH $A\ ^2\Sigma^+$ (v', N') quantum state, the latter limited to vibrational state v'=0 and various rotational levels N' in the F_1 spin-rotation manifold for this review. The temperature and rotational level dependencies of the rate coefficients are similar for many quenching partners.(4, 5, 39) These trends are illustrated in Figure 2 using the extensive data available for the simplest molecular quencher, namely H_2. Specifically for H_2, σ_Q decreases with increasing temperature over the range from 200 to 1200 K with a value of 8.7 $Å^2$ at 298 K.(5, 32-35) The temperature-dependent trend is captured using an empirical form proposed by Henderson and Heard.(5) At yet lower temperatures sampled in studies performed in this laboratory, the quenching cross section would then be expected to be even larger than that at 200 K. The negative temperature dependence indicates that the quenching process involves an attractive interaction between the OH $A\ ^2\Sigma^+$ and H_2 partners. As discussed later, theory has shown that an attractive interaction guides the collision pair to regions of strong nonadiabatic coupling that lead to removal of OH A $^2\Sigma^+$ population.

The quenching cross section σ_Q also decreases with increasing rotational level N' in the excited OH $A\ ^2\Sigma^+$ state at room temperature, as shown in Figure 2 for H_2.(40, 41) This trend has been interpreted as follows: Increasing rotational excitation leads to averaging over OH orientation in the collisional encounter, thereby averaging over a strongly anisotropic interaction with respect to OH orientation. Again, as presented later, theoretical calculations have shown that only specific orientations of OH with respect to H_2, namely with the O-side of OH pointing toward OH, are effective in quenching.

III. Experimental Methods

Recent experiments in the Lester laboratory have focused on characterizing the products from collisional quenching of OH $A\ ^2\Sigma^+$ in order to gain insight into the quenching mechanism.(12-23) The experimental studies utilize a pump-probe technique illustrated in

Figure 1 to examine the products of collisional quenching events. Hydroxyl radicals are generated in the throat of a pulsed supersonic jet expansion by the 193 nm photolysis of nitric acid vapor entrained in a 20-30% mixture of the quenching partner in helium. An ultraviolet pump laser prepares OH with purely electronic excitation in the v'=0, N'=0 level of the excited $A\ ^2\Sigma^+$ state (4.02 eV) in the collisional region of the expansion. Both the initial N'=0 level and low temperature in the expansion (average collision energy of ~0.025 eV)(20) are expected to give rise to large quenching cross sections based on prior kinetic measurements. For example, when H_2 is introduced into the carrier gas mixture (30% H_2 in He), the OH $A\ ^2\Sigma^+$ (v'=0, N'=0) fluorescence lifetime decreases from its radiative value to τ=180 ns and Φ is reduced to 0.26 under representative experimental conditions shown in Figure 3 as a result of significant quenching by H_2; note that He is ineffective in quenching OH. After a short time delay, a spatially overlapped probe laser is used to interrogate the products following quenching under single collision conditions.(17) Nonreactive and reactive quenching products require different probe laser schemes, which are discussed below.

Nonreactive quenching by a collision partner, M, returns OH $A\ ^2\Sigma^+$ to its ground $X\ ^2\Pi$ state. The probe laser in these experiments utilize the OH *A*-*X* band system with LIF detection as a highly sensitive and selective method to map out the rovibrational (v''=0-2, N'') and fine-structure resolved product state distribution.(12-19) The fine-structure refers to the spin-orbit manifold, F_1 or F_2, and Λ-doublet state, $\Pi(A')$ or $\Pi(A'')$. The product state distributions are obtained by measuring the probe LIF intensities, initially scaled to a reference line, for each OH $X\ ^2\Pi$ product state. Under saturated LIF conditions, these relative intensities can be converted to relative populations after accounting for the fluorescence lifetimes and quantum yields of the OH $A\ ^2\Sigma^+$ (v',N') levels accessed by the probe transitions, the degeneracies of the upper and lower states, and the detection sensitivity, particularly the bandpass filters used in collecting fluorescence.

An important aspect of these studies is determining the branching fraction to nonreactive quenching, in particular OH $X\ ^2\Pi$ (v''=0-2, N''). In this case, the relative intensity of the very intense pump LIF signal is directly compared to the much weaker probe LIF signals for selected product states; the relative intensities are then converted to relative populations. This

measurement allows fractional populations, defined as the fraction of initially excited OH $A\ ^2\Sigma^+$ (v'=0, N'=0) that populates a particular OH $X\ ^2\Pi$ (v''=0-2, N'') product state, to be determined. Typically, the experimental population distribution is fit to a few parameter functional form in order to estimate population in unobserved levels. By summing over product states, the total branching fraction to nonreactive quenching is determined.(13) Analogous branching fraction measurements have been made for quenching of NO $A\ ^2\Sigma^+$ (v'=0) to NO $X\ ^2\Pi$ (v''=0) by O_2, CO, CO_2, and H_2O via ground state recovery measurements.(42)

Reactive quenching of OH $A\ ^2\Sigma^+$ (v'=0, N'=0) prepared by the pump laser results in reaction products being generated. In the systems discussed below, H-, D- and O-atom products are formed with molecular cofragments.(20-23) Briefly, H-atoms resulting from reactive quenching of OH $A\ ^2\Sigma^+$ (v'=0, N'=0) are probed using two-photon excitation and collection of the subsequent Lyman-α fluorescence. By scanning the wavelength of the probe laser, the Doppler profiles of the H-atoms are measured; the integrated intensity reflects population in the H-atom product channel. The Doppler profiles yield information regarding the translational energy distribution of the H-atom products and associated internal energy of the molecular cofragment. Transformation from a Doppler profile to a product translational energy, $P(E_T)$, distribution can be carried out by fitting the profile to a Gaussian distribution. The fwhm of the distribution can be directly related to a translational temperature assuming a Boltzmann distribution.(43) An alternative rigorous transformation was used for Doppler profiles with more complicated lineshapes.(23) A two-photon LIF probe scheme is similarly applied to study O-atom products with fine-structure resolution; however, the smaller Doppler shift for the heavier atom prevents Doppler profiles from being obtained at the experimental laser resolution. Experimental observation of O-atoms following reactive quenching of OH $A\ ^2\Sigma^+$ (v'=0, N'=0) by different molecular partners reflects population in that product channel.

Some other experimental methods have been used to probe the outcomes of collisional quenching. Ortiz-Suarez *et al.* used a fixed source, rotatable detector crossed molecular beam apparatus to investigate reactive quenching of OH $A\ ^2\Sigma^+$ by D_2 at a much higher collision energy of 0.16 eV.(24) While the pump step is the same as that above, the probe step involves a Rydberg tagging time-of-flight method of the D-atoms generated under single collision

conditions from reactive quenching. The time-of-flight spectra and angular distribution of the tagged D-atoms are recorded and transformed into center-of-mass translational energy distributions, which gives information regarding the internal energy of the molecular cofragment. Another promising technique for examining the outcomes of quenching is IR emission from vibrationally excited products, as demonstrated in work by Hancock and coworkers on quenching of NO $A\ ^2\Sigma^+$ by NO, N_2O and CO_2.(44, 45)

IV. Outcomes from Nonreactive Quenching

A. Branching to Nonreactive Quenching

The branching to nonreactive quenching varies greatly depending on the collision partner, yet there is no a priori way to predict the branching ratio. As shown in Figure 4, the percentage of quenching collisions which returns OH to its ground $X\ ^2\Pi$ electronic state in v''=0-2 ranges from nearly 100% to 0%. Quenching of OH $A\ ^2\Sigma^+$ (v'=0, N'=0) by Kr results in 95% of products detected in the nonreactive quenching pathway.(19) Quenching collisions with N_2 also overwhelmingly results in nonreactive quenching [≥88%].(18) The small balance is thought to appear in yet higher rotational states that could not be probed by LIF due to rapid electronic predissociation of the upper state. Reactive quenching pathways have not been detected.(46)

The branching fraction measurements for quenching collisions of OH $A\ ^2\Sigma^+$ (v'=0, N'=0) with CO_2 and O_2 also show significant population in the nonreactive quenching pathway, 62% and 40% respectively.(15) However, a large portion of quenched population is not observed. This could indicate OH $X\ ^2\Pi$ population in yet higher vibrational and/or rotational levels that cannot be detected by LIF. However, a more likely explanation is that reactive quenching is significant in these systems, as demonstrated in a later investigation with O_2 as the collision partner.(20)

Nonreactive quenching is only a minor pathway with H_2 or D_2 as the collision partner [12% and 15%, respectively].(14) Furthermore, quenching of OH $A\ ^2\Sigma^+$ (v'=0, N'=0) by CO did not result in observable OH $X\ ^2\Pi$ (v'', N'') products from nonreactive quenching.(20) Reactive quenching pathways in these systems clearly dominate the quenching mechanism as discussed below.

B. OH $X\,^2\Pi$ Vibrational Distributions

The branching to nonreactive quenching can be further broken down into the branching to specific OH $X\,^2\Pi$ vibrational levels, shown in Figure 4. The overwhelming trend for these quenching partners is that OH $X\,^2\Pi$ is produced primarily in v''=0 with significantly less population in v''=1 and even less in v''=2. Given this trend, we will discuss the vibrational distributions for these collision partners as a whole. On average, ~75% of the nonreactive quenching events produce OH $X\,^2\Pi$ in v''=0. Typically, less than 20% of nonreactive quenching products are produced in v''=1. In the OH + H_2/D_2 systems, a small amount of population was observed in v''=2, accounting for less than 5% of the nonreactive quenching outcomes.(14) The predominant population of OH $X\,^2\Pi$ (v''=0) upon quenching is indicative of a small change in OH bond length from the excited electronic state through regions of nonadiabatic coupling to ground state products.

C. OH $X\,^2\Pi$ Rotational Distributions

The OH $X\,^2\Pi$ product rotational distributions were probed with rovibrational and fine-structure resolution following nonreactive quenching of OH $A\,^2\Sigma^+$ with the collision partner of interest. Only the OH $X\,^2\Pi$ (v''=0, N'') distributions are discussed here; the v''=1 distributions are very similar. In each system, the OH $X\,^2\Pi$ product rotational distribution was fit to a simple functional form, and these fits are shown in Figure 4. Overall, a large degree of OH $X\,^2\Pi$ rotational excitation results from collisional quenching.

For nonreactive quenching of OH $A\,^2\Sigma^+$ (v'=0, N'=0) by Kr, the OH $X\,^2\Pi$ (v''=0, N'') distribution exhibits a peak at N''~9, followed by a slight dip and then a second peak N''~17.(19) The average rotational energy is $\langle E_{rot}(v''=0)\rangle$ = 4400 cm^{-1}. The doubly peaked rotational distribution in the OH + Kr system is different than other systems studied, although there is still an overall high degree of rotational excitation.

Quenching of OH $A\,^2\Sigma^+$ (v'=0, N'=0) by N_2 exhibits an even higher degree of rotational excitation.(18) The rotational distribution is broad, increasing to a peak at N''=18, and then gradually falling off to higher energy. Population was detected out to N''=27, beyond which

rapid predissociation in the OH $A\ ^2\Sigma^+$ state used for LIF detection prevented probing higher rotational levels. The average rotational energy of this highly nonstatistical distribution is $\langle E_{rot}(v''=0)\rangle$ = 6540 cm^{-1}.

Quenching of OH $A\ ^2\Sigma^+$ (v'=0, N'=0) by CO_2 results in a more moderate degree of rotational excitation.(15) The rotational distribution peaks at N''=5. The average rotational energy is $\langle E_{rot}(v''=0)\rangle$ = 1840 cm^{-1}, which is lower than the other systems studied by about 3000 cm^{-1}. This distribution, unlike other systems, can be well characterized by a rotational temperature of ~2250 K.

Quenching of OH $A\ ^2\Sigma^+$ (v'=0, N'=0) by O_2 is again nonthermal and shows a large degree of rotational excitation.(15) The product rotational distribution increases to a peak at N''=17. This distribution has $\langle E_{rot}(v''=0)\rangle$ = 4780 cm^{-1}.

Quenching of OH $A\ ^2\Sigma^+$ (v'=0, N'=0) by H_2 and D_2 results in very similar degrees of high rotational excitation.(13, 14, 16) The OH $X\ ^2\Pi$ distribution peaks around N''= 15 and N''=17 following quenching by H_2 and D_2, respectively. The average rotational energy in the OH + H_2 system was found to be $\langle E_{rot}(v''=0)\rangle$ = 4480 cm^{-1}, after including several higher rotational levels measured later in Ref. (13) and reanalyzed in Ref. (17). The average rotational energy was only slightly higher in the OH + D_2 system at $\langle E_{rot}(v''=0)\rangle$ = 4600 cm^{-1}.

The extent of rotational excitation across the range of diatomic quenching partners (and Kr) cannot be understood from a purely kinematic perspective. If the collision partner is assumed to be structureless, the degree of rotational excitation in the OH $X\ ^2\Pi$ products would scale with the reduced mass of the system, Kr > O_2 > N_2 > D_2 > H_2,(14) which differs considerably from the observed trend. The high degree of OH $X\ ^2\Pi$ product rotational excitation seen in most systems is a signature that reflects the mechanism for quenching as discussed later.

D. OH $X\ ^2\Pi$ Fine Structure Distributions

For each system investigated, all four OH $X\ ^2\Pi$ fine structure components were probed for at least a subset of N'' levels. Across these systems, the F_1 and F_2 spin-orbit levels were

equally populated for a given *N*".(14, 15, 17-19) This lack of spin-orbit preference shows that in the generation of rotational angular momentum, both vector couplings with electron spin are equally probable.

The propensity for populating specific Λ-doublet states was also investigated. In the high *N* limit, the Λ-doublet population reflects the alignment of the orbital containing the unpaired electron either parallel [$\Pi(A')$] or perpendicular ([$\Pi(A'')$] to the plane of OH nuclear rotation. Only the OH + H_2, including its isotopic variants, and OH + N_2 systems showed any significant degree of orbital alignment.(14, 18) In both cases, OH $X\,^2\Pi$ is formed preferentially in the $\Pi(A')$ Λ-doublet with the half-filled pπ orbital lying in the OH rotation plane. This propensity will be discussed later and linked to properties of the potentials involved in the quenching mechanism.

V. Outcomes from Reactive Quenching

Reactive quenching is defined as those collisional quenching processes that result in new products being formed. The energy available to the products, E_{avl}, is defined as $E_{avl} = E_{h\nu} - \Delta H_{rxn} + E_{coll}$, where $E_{h\nu}$ is the excitation energy, ΔH_{rxn} is the reaction enthalpy, and E_{coll} is the collision energy. Of the collision partners discussed in the previous sections, quenching of OH $A\,^2\Sigma^+$ by CO_2, O_2, H_2/D_2, and CO result in a significant fraction of products in reactive channels based on the branching fraction measurements presented in Section IV A. The studies described here focus on reactive quenching pathways that yield atomic products, specifically H, D, or O atoms.

Reactive quenching of OH $A\,^2\Sigma^+$ by O_2 accounts for up to 60% of quenching outcomes.(15) There are several possible reactive products that are energetically accessible from the OH $A\,^2\Sigma^+ + O_2$ asymptote, including H $^2S + O_3$. For this channel, the resultant P(E_T) distribution shown in Figure 5 spans the 0.68 eV of E_{avl} with $\langle E_T \rangle$ = 0.25 eV, indicating that ~35% of E_{avl} goes into product translation.(20) The product translational energy distribution is similar to that of a statistical process, that is, the excess energy appears to be randomized in the OH-O_2 collision pair. Direct comparison of the H-atom yield from quenching of OH $A\,^2\Sigma^+$ by

O_2 and H_2,(20, 21, 23) indicates that ~12% of quenching collisions result in H + O_3 products. The remainder of the quenched products (~48%) follows the O ^3P + HO_2 (*X*, *A*) (E_{avl} = 1.69 eV, 0.82 eV) pathway. The O-atom products are detected with a statistical ^3P_J fine structure distribution, but possible electronic and/or internal excitation of the HO_2 fragment could not be determined.(20)

Reactive quenching of OH $A\ ^2\Sigma^+$ by H_2 results in formation of H + H_2O products (E_{avl} = 4.72 eV). Reactive quenching is the dominant contribution (~88%); only 12% follows the nonreactive quenching pathway. The derived P(E_T) distribution is highly nonstatistical, as shown in Figure 5.(21-23) The distribution exhibits a prominent peak at low translational energy (below 0.5 eV), accounting for 60% of the reactive products. A secondary, broader feature is evident at higher translational energy, peaking at ~2.6 eV, with a tail that extends to the energetic limit. The average product translational energy is 0.84 eV or 18% of E_{avl}. The balance of the excess energy flows into H_2O internal energy, resulting in highly excited 'hot' water products.

The deuterated variants of this system have also been studied. Quenching of OD $A\ ^2\Sigma^+$ by H_2 generates H + HOD and D + H_2O products.(23) Quenching of OH $A\ ^2\Sigma^+$ by D_2 to form D + HOD and H + D_2O products yields analogous results,(22, 23) albeit with H- and D-atom findings reversed. For OD $A\ ^2\Sigma^+$ + H_2, the primary H + HOD channel accounts for 75% of the reactive quenching outcomes; the secondary D + H_2O channel is also notable with 25% of outcomes. The highly nonstatistical P(E_T) distribution for H + HOD products exhibits a strong peak at low translational energy (below 0.5 eV) and a long tail extending to the energetic limit as shown in Figure 5. The H + HOD products have an average translational energy of 0.48 eV, which corresponds to 10% of E_{avl}. By contrast, the D + H_2O channel exhibits a small peak at low product translational energy (below 0.5 eV), a distinctive secondary peak at ~1.8 eV, and then falls off toward the energetic limit. The D + H_2O products have an average translational energy of 0.82 eV, corresponding to 18% of E_{avl}. This secondary pathway for quenching is attributed to an insertion-like process since the O from OD appears to insert into the H_2 bond to form D + H_2O products. The distinctive peak at higher translation energy is associated with this process.

Adding together the $P(E_T)$ distributions for the H + HOD and D + H_2O channels from OD $A\ ^2\Sigma^+$ + H_2 yields a total $P(E_T)$ distribution which is similar to that found for quenching of OH $A\ ^2\Sigma^+$ by H_2.

Ortiz-Suarez *et al.* used crossed molecular beam scattering at significantly higher collision energy to study reactive quenching of OH $A\ ^2\Sigma^+$ by D_2 forming D + HOD.(24) The D-atom products were found to be predominately forward scattered with a minor backward scattering component relative to the incident D_2. The angular scattering distribution indicates a direct mechanism in which OH $A\ ^2\Sigma^+$ abstracts a D-atom from D_2 at relatively large impact parameters and the newly formed HOD continues in the same direction as the incident OH $A\ ^2\Sigma^+$ beam. Their kinetic energy distribution for the D-atom products peaks at ~0.55 eV with an average product translational energy of 0.8 eV. This corresponds to 16% of E_{avl}, consistent with a large fraction of E_{avl} (~84%) released as internal excitation of the water product. The change in the $P(E_T)$ distribution compared to Ref. (23) may reflect a strong dependence of quenching on collision energy.

Finally, reactive quenching of OH $A\ ^2\Sigma^+$ by CO can result in H + CO_2 (E_{avl} = 5.08 eV) and O + HCO (E_{avl} = 0.23 eV) products; no OH $X\ ^2\Pi$ (v''=0-1, N'') products from nonreactive quenching are detected.(20) A branching fraction measurement, directly comparing the H-atom yield from quenching of OH $A\ ^2\Sigma^+$ by CO and H_2,(20, 21, 23) indicates that ~1/4 of quenching collisions result in H + CO_2. A similar comparison of the O-atom yield from quenching of OH $A\ ^2\Sigma^+$ by CO and O_2 shows that ~3/4 follows the O + HCO pathway. For the H + CO_2 channel, the nonstatistical $P(E_T)$ distribution is peaked at low translational energy release with an average energy of 0.29 eV. Only ~6% of E_{avl} goes into product translation, leaving nearly 4.8 eV on average as highly internally excited CO_2. The O-atom products exhibit a statistical ^3P_J fine structure distribution; no information is obtained on possible internal excitation of the HCO fragment.

VI. Theoretical Exploration of OH $A\ ^2\Sigma^+$ Quenching by Molecular Partners

A. General Considerations

The Born-Oppenheimer Approximation (BOA) is the cornerstone for studying chemical processes through quantum mechanics. The separation of electronic and nuclear motion, made possible by neglecting the first and second derivatives of the electronic wavefunction with respect to the nuclear coordinates, allow for heavy nuclei to move on a single potential energy surface created by the much faster moving electrons. However, when potentials approach each other closely, the coupling between the nuclear and electronic motion becomes important and the BOA breaks down. This coupling, often called derivative or nonadiabatic coupling, is defined in terms of the change in the electronic wavefunction with respect to nuclear coordinates divided by the energy difference between the electronic states.(6) The breakdown of the BOA is ubiquitous, especially in larger systems, and allows for nonadiabatic events to take place in regions of strong coupling known as conical intersections (CI).(8-11)

In a molecular system with N internal degrees of freedom, degeneracy between electronic states will be found in a subspace of N-2 dimensions.(47) The nuclear coordinates that linearly lift the degeneracy define a "branching space" with associated vectors known as the energy difference (or tuning) coordinate **g** and the interstate coupling coordinate **h**.(48-50) When plotted in these two nuclear coordinates, the CI resembles a double cone and hence the name conical intersection.(51) The topography and the tilt of the cone are illustrated for the OH + H_2 system in Figure 6, along with the **g** and **h** vectors superimposed on the geometric configuration at this CI.(26) The remaining N-2 dimensions in which the degeneracy is maintained form a "seam" of CI. This seam is made up of an infinite number of CIs; the lowest energy CI is called the minimum energy crossing (MEX).

Much attention has been focused on understanding the regions at or near points of CI. (8-11) Derivative couplings between the electronic states are very strong in the vicinity of the CI (and infinitely large at the point of CI), which enables these regions to have a profound effect on nuclear dynamics. CIs allow for population to be funneled from one electronic potential to another, opening up nonradiative decay pathways. In the examples that follow, electronic quenching occurs via passage through regions of CI. This review is not intended to be an

exhaustive study of the theoretical treatment of conical intersections, but rather a focused look in Section VI. B. at the local forces in the vicinity of CIs relevant to quenching in OH $A\ ^2\Sigma^+$ + M systems for M = H_2, N_2, and CO; no theoretical studies are currently available for M = O_2 and CO_2. (Theoretical studies for M = Kr have recently been undertaken,(19) but are not presented in detail here.) In addition, theoretical advances are allowing for dynamical calculations that include these regions of strong coupling for OH $A\ ^2\Sigma^+ + H_2$ as outlined in Section VI. C. For a more detailed review of conical intersections, including relevant mathematical formulae and more complete references on the subject, we point the reader to several other reviews on this topic.(8-11)

B. Regions of Conical Intersection for OH $A\ ^2\Sigma^+ + H_2$, N_2 and CO

This section focuses on the local forces in the CI regions relevant to quenching of OH $A\ ^2\Sigma^+$ by H_2, N_2 and CO. The earliest *ab initio* calculations by Walch in 1997 revealed a CI region in a C_{2v} HO-H_2 configuration,(25) accessible in a barrierless path from the OH $A\ ^2\Sigma^+ + H_2$ asymptote when the O-side of the OH radical points toward the H_2 as shown in Figure 1. Reversing the orientation of OH $A\ ^2\Sigma^+$, such that the H-side of the OH radical points toward H_2, leads to an attractive well region,(52, 53) previously probed in spectroscopic studies of the OH-H_2 pre-reactive van der Waals complex,(25, 54-56) but not to the CI region and quenched products. Significant barriers to internal rotation of OH on the excited state surface limit access to the CI region to OH $A\ ^2\Sigma^+ + H_2$ collisions with the O-side of OH directed toward H_2.

In 2000, Hoffman and Yarkony carried out electronic structure calculations for quenching of OH $A\ ^2\Sigma^+$ by H_2 that identified representative points along seams of CI in C_{2v}, $C_{\infty v}$, and C_s configurations,(26) building on earlier work,(57, 58) in each case with the O-side of OH pointing toward H_2, but with H_2 in any possible orientation with respect to OH. These seams can be accessed in a barrierless path from the OH $A\ ^2\Sigma^+ + H_2$ asymptote. In addition, they mapped out the topography in the vicinity of the CI and defined the unique **g**-**h** branching plane from which the potentials separate linearly.(26) For the OH + H_2 MEX shown in Figure 6, the energy difference gradient **g** vector drives the OH and H_2 moieties toward (+**g**) or away (–**g**) from one another as they approach and exit from the CI. The +**g** vector leads toward reactive

quenching, while the –**g** vector promotes the nonreactive quenching channel. The interstate coupling **h** vector puts a torque on the OH radical in the vicinity of the CI, likely giving rise to the significant rotational excitation of the OH X $^2\Pi$ products from nonreactive quenching.

For the OH ($A\ ^2\Sigma^+$, $X\ ^2\Pi$) + N_2 system, *ab initio* calculations by Walch in 1997 identified a barrierless path from the OH $A\ ^2\Sigma^+$ + N_2 asymptote with the O-side of OH pointing toward N_2 to a CI in a linear HO-N_2 configuration.(25) This CI region was ascribed as the critical region for quenching. [The lower dimensional OH + Kr system is similar, with calculations indicating that only the O-side of OH interacting with Kr results in quenching.(19)] In 2009, Matsika performed further electronic structure calculations for the OH ($A\ ^2\Sigma^+$, $X\ ^2\Pi$) + N_2 system focused on characterizing the region of conical intersection, specifically the **g**/**h** branching space and topography of the CI.(18) The Cartesian representations of the **g** and **h** vectors for HO-N_2, shown in Figure 6 of Ref. (18), are remarkably similar to those for HO-H_2 (Figure 6). In both systems, the interstate coupling vector, **h**, places a torque on the OH moiety as it moves through the region of CI, which is qualitatively linked to the large degree of rotational excitation of the OH $X\ ^2\Pi$ products observed experimentally. The HO-N_2 system differs in having a significant tilt of the cone toward the –**g** direction, which drives the OH and N_2 species away from one another after passing through the CI. The tilt favors the nonreactive quenching channel, which is the only channel seen experimentally.

The OH ($A\ ^2\Sigma^+$, $X\ ^2\Pi$) + CO system was originally investigated via electronic structure calculations and classical trajectory studies in 1988.(59, 60) While the earlier work mapped out regions of the excited state surface with strong nonadiabatic coupling, a more recent theoretical study(20) has taken advantage of the significant advances in algorithms(49, 61) to identify and characterize points of conical intersection between states of the same symmetry. The geometric configurations, energy difference gradients, and interstate couplings for four MEXs were identified. Three of these intersections occur when the oxygen side of OH points toward CO. Since this system proceeds dominantly to reactive quenching, these three regions of intersection likely lead to the formation of H + CO_2, which was experimentally determined to account for 25% of quenching outcomes. The **g** and **h** vectors [see Figure 6 of Ref. (20)] suggest

that CO_2 products would be vibrationally excited, consistent with the minimal translational energy seen experimentally.

Interestingly, the OH + CO system was the first instance where a conical intersection accessible from the OH $A\ ^2\Sigma^+$ + M asymptote has been found when the H-side of OH points towards its quenching partner. Moreover, a barrierless path has been identified along a seam of conical intersection that drives OC + HO toward reaction, forming HCO + O products. The dominant HCO + O product channel (75% of quenching outcomes) has been attributed to the presence of this seam of intersection. In this case, the **g** vector suggests that the HCO products could be formed with bend excitation.

C. Dynamical Calculations of Quenching for OH $A\ ^2\Sigma^+ + H_2$

This section describes dynamical calculations for quenching of OH $A\ ^2\Sigma^+$ by H_2, and the potentials developed for such applications. In 2007, Kłos and Alexander carried out extensive calculations to explore the potentials (planar) for the lowest states of A′ (1A′ and 2A′) symmetry correlating with OH ($A\ ^2\Sigma^+$, $X\ ^2\Pi$) + H_2 as well as the fully repulsive state of A″ (1A″) symmetry derived from OH $X\ ^2\Pi$ + H_2.(16) The A′ surfaces couple together at the CI region. The potentials reveal steep gradients away from the HO-H_2 CI region as a function of both OH orientation and intermolecular distance. These angular forces will lead to rotational excitation of the electronically quenched OH products, as seen experimentally. Additionally, assuming the dynamics favor passage through the CI in planar geometries, the highly rotationally excited OH products would be expected to emerge primarily in the Π(A′) Λ-doublet level, as observed experimentally.

In 2010, Bowman and coworkers carried out classical trajectory studies to explore the outcomes of collisional quenching of OH $A\ ^2\Sigma^+$ by H_2 by examining the post-quenching dynamics initiated at various points along the seams of CI.(17, 27, 28) The initial momenta were sampled partially microcanonically, corresponding to a diabatic model for the dynamics. Trajectories were propagated on full dimensional, electronically adiabatic potentials to predict the properties of the products.

The OH $X\,^2\Pi$ products from nonreactive quenching are predicted to have a substantial degree of rotational excitation and little vibrational excitation, in good agreement with experimental results.(17, 27, 28) Specifically, nonreactive quenching of OH/D $A\,^2\Sigma^+$ by H_2 yields an experimental product rotational distribution for the most populated v''=0 level that peaks at N''~15 for OH $X\,^2\Pi$ and N''~21 for OD $X\,^2\Pi$. In both cases, the trajectory calculations show similar rotational distributions peaked at even higher rotational excitation and slightly warmer vibrational distributions for the OH and OD $X\,^2\Pi$ products. The as yet unobserved H_2 products of nonreactive quenching are also predicted to have significant vibrational excitation in v_{H_2}=1 and 2.

The trajectory calculations predict a branching ratio that strongly favors reactive quenching with a reactive to nonreactive branching ratio of 70:30.(27, 28) This is in accord with experimental branching fraction measurements which also show nonreactive quenching to be the minor pathway ($\leq$ 20%).(14) The calculations predict that reactive quenching proceeds via an abstraction mechanism nearly exclusively with only a small contribution from insertion. Representative trajectories of these processes(17) are available online.(62) However, experiments utilizing isotopic labeling clearly show a much more substantial role of insertion leading to H-atom products from OH $A\,^2\Sigma^+ + D_2$ and D-atom products from OD $A\,^2\Sigma^+ + H_2$.(22, 23)

The trajectory calculations predict the H/D-atom translational energy distributions for the OH $A\,^2\Sigma^+ + H_2$ and D_2 abstraction pathways,(27, 28) peaked at 0.4 and 0.8 eV, respectively, which are somewhat higher than determined experimentally.(21-23) Quite interestingly, the calculations indicate a high probability of bend excitation (up to 19 quanta!) for the very highly vibrationally excited H_2O or HOD products.(28) A lesser degree of symmetric and asymmetric stretch excitation of the H_2O or HOD products is also predicted. The high degree of vibrational excitation for the 'hot' water products can be understood by comparing the geometric properties of HO-H_2 at the CI region(26) with the equilibrium structure of the H_2O product. The HOH bond angle is highly extended at the CI, resulting in a large degree of bend excitation of the H_2O product. In addition, the newly formed OH bond is elongated at the CI, resulting in OH stretch excitation of the water product.

Experimental studies of OH $A\ ^2\Sigma^+$ + H_2 reactive quenching in the Hancock group are utilizing FTIR emission to characterize the quantum state distribution of the vibrationally excited H_2O products, which may be even hotter than theoretical predictions.(63) Most recently, Bowman and coworkers have reexamined the quantized vibrational distribution of the H_2O products. They focused on the overtone bending distribution and its combination with different asymmetric stretch states, the latter having large IR emission oscillator strength.(64)

In 2010, Han and coworkers in 2010 reported time-dependent wave-packet calculations of the nonadiabatic quenching dynamics for OH $A\ ^2\Sigma^+$ by H_2 and D_2 on the 1A′ and 2A′ potentials restricted to a plane.(29, 30) They computed integral cross sections for the reactive and nonreactive quenching channels and quantum state distributions for the nonreactive channel. They found a high degree of rotational excitation of the quenched OH $X\ ^2\Pi$ products, as observed experimentally, and also predict highly vibrationally excited H_2 (up to v_{H_2} =6) products (not yet observed). Interestingly, their calculations indicate substantial changes in the integral cross sections with collision energy.

More recently, Collins, Zhang, and coworkers have constructed diabatic potentials for the three electronic states of OH ($A\ ^2\Sigma^+$, $X\ ^2\Pi$) + H_2.(31) They have utilized surface-hopping classical trajectories of the quenching dynamics at collision energies commensurate with the crossed beam study of Ortiz-Suarez *et al.*,(24) and obtain good agreement in the distributions of kinetic energy and scattering angle to HOD + D products. In ongoing work, Truhlar, Bowman and coworkers are also developing new diabatic potentials and couplings for OH ($A\ ^2\Sigma^+$, $X\ ^2\Pi$) + H_2,(65) which are expected to facilitate simulations of the electronically nonadiabatic collision dynamics. Finally, Dillon and Yarkony have recently identified an additional pathway for reactive quenching of OH $A\ ^2\Sigma^+$ + H_2,(66) which may be the origin of the insertion mechanism seen experimentally. Portions of the path are nonplanar, facilitating the formation of three equivalent OH bonds of H_3O, which could break and yield H-atom products.

VII. Conclusions

The electronic quenching of OH $A\ ^2\Sigma^+$ has been investigated for many molecular partners of importance in atmospheric and combustion environments. The outcomes of these

collisional quenching events provide experimental observables that reflect on the nonadiabatic coupling as the system evolves to nonreactive or reactive products. The general trends observed are summarized here. The large cross sections for collisional quenching are indicative of fast dynamics and strong coupling between the OH ($A\ ^2\Sigma^+$, $X\ ^2\Pi$) + M potentials in very limited regions, e.g. O-side of OH pointing toward M, of the available configuration space. The minimal vibrational excitation of the OH $X\ ^2\Pi$ products shows that the OH bondlength is essentially unchanged as it switches from the excited $A\ ^2\Sigma^+$ to ground $X\ ^2\Pi$ electronic state. On the other hand, the quite significant rotational excitation of the OH $X\ ^2\Pi$ products is indicative of a strong torque placed on the OH radical in the vicinity of the CI; for N_2 and H_2 collision partners, this torque is readily apparent from the interstate coupling vector **h**. In these same systems, the $\Pi(A')$ Λ-doublet propensity of the OH $X\ ^2\Pi$ products appears to reflect the A' symmetry of the potentials at the crossing. The kinetic energy release to H, D, and O-atom reaction products and the corresponding internal energy of the cofragment provides additional insight on the geometric configuration at the CI, particularly when it differs greatly from the equilibrium structure of the products. In some cases, such as the H_2O products from OH $A\ ^2\Sigma^+$ + H_2, the configuration at the CI maps onto highly vibrationally excited products. Finally, the pitch and tilt of the cone at the intersection influences the branching between nonreactive and reactive quenching events. Still needed are quantum scattering and/or classical dynamics calculations to evaluate quenching cross sections, branching between multiple reactive and nonreactive product channels, as well as the quantum state and kinetic energy distributions of the products. Such studies are underway by several theoretical groups for the benchmark systems described here.

Acknowledgements

MIL thanks the many graduate students and postdoctoral researchers who contributed to the experimental aspects of this research and are cited in this review. In addition, MIL thanks Millard Alexander, Joel Bowman, Tom Stephenson, and David Yarkony for many insightful discussions on nonadiabatic dynamics. The experimental research was principally supported by the U.S. Department of Energy, Basic Energy Sciences (DE-FG02-87ER13792).

Partial equipment support was provided by the Chemistry Division of the National Science Foundation.

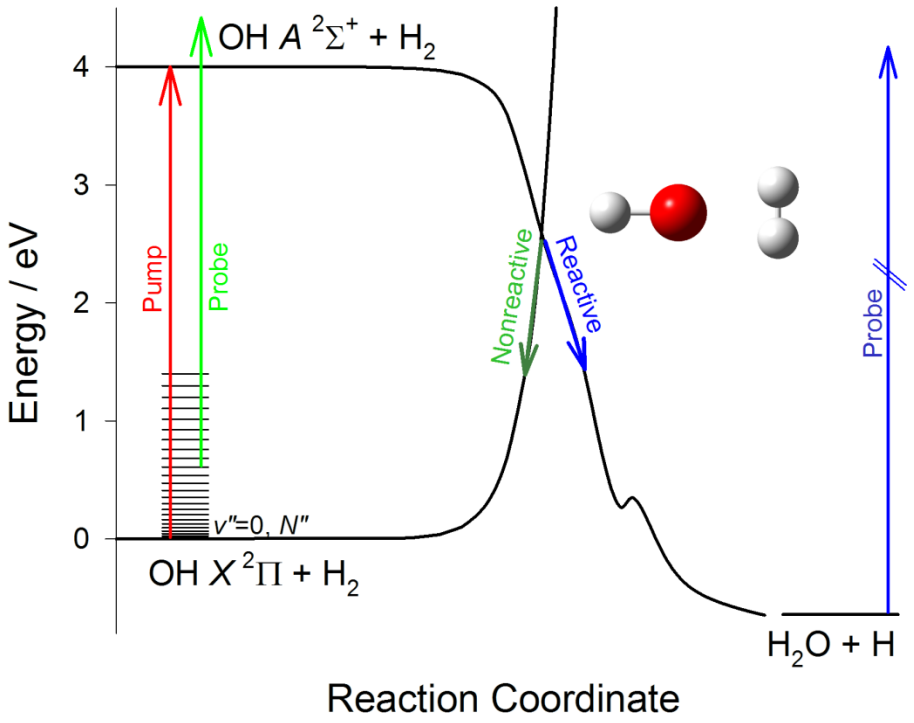

Figure 1. Simplified reaction coordinate for quenching of OH *A* $^2\Sigma^+$ by H_2 [adapted from Ref. (25)] via the C_{2v} HO-H_2 conical intersection [from Ref. (26)]. Both nonreactive quenching producing OH *X* $^2\Pi$ + H_2 and reactive quenching to H_2O + H are illustrated. The pump excitation that prepares OH *A* $^2\Sigma^+$ (*v*′=0, *N*′=0) and probe schemes utilized for detection of the quenched OH *X* $^2\Pi$ and H-atom products are indicated.

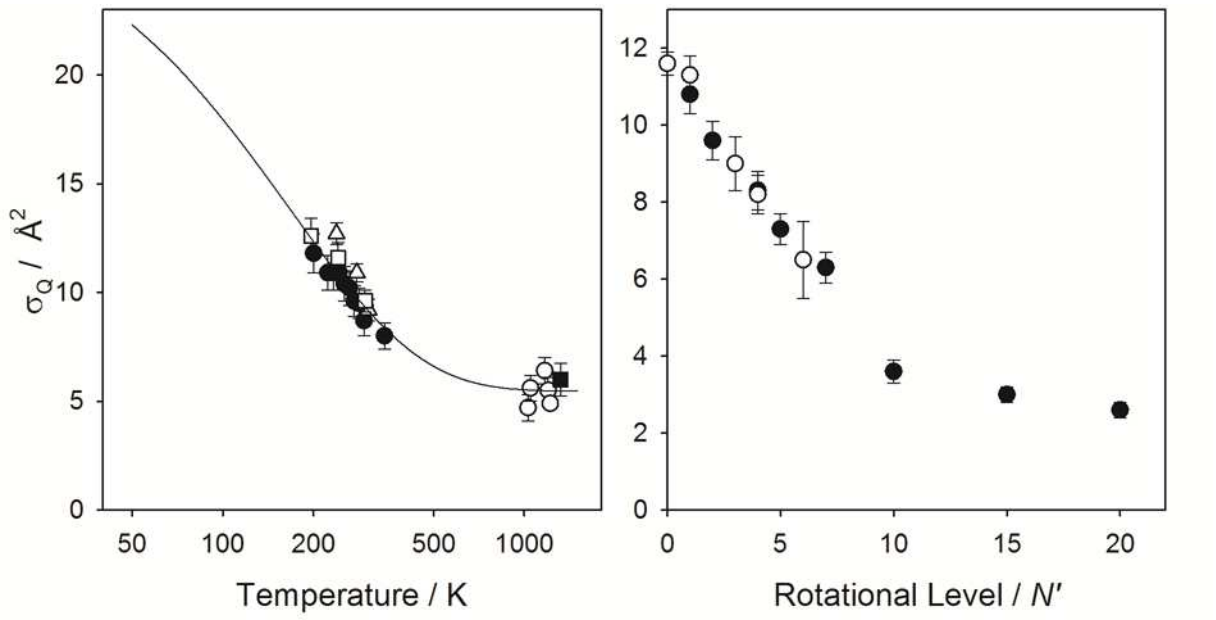

Figure 2. Cross sections σ_Q for quenching of OH $A\ ^2\Sigma^+$ (v'=0, N') by H_2 are shown as a function of temperature and initial rotational level N' with data from Refs. (5, 40, 41). The temperature-dependent trend is modeled by an empirical relationship proposed by Henderson and Heard in Ref. (5).

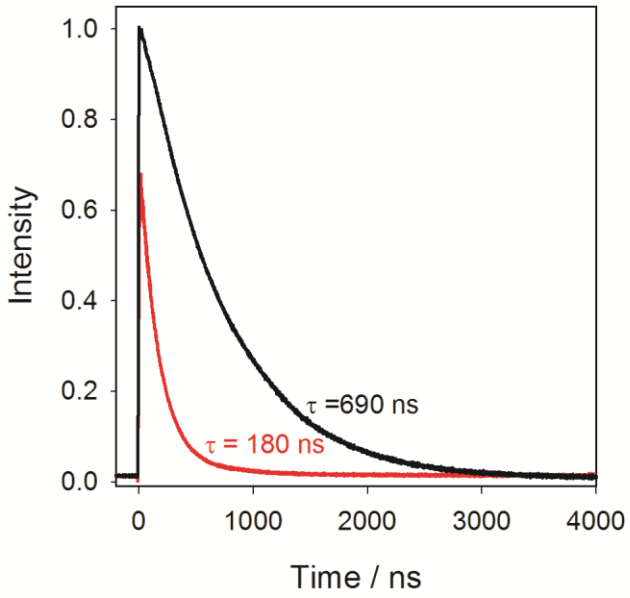

Figure 3. Fluorescence decays for OH $A\ ^2\Sigma^+$ (v'=0, N'=0) in a pure He carrier gas (black) and 30% H_2 in He gas mixture (red) under similar experimental conditions. The decreased fluorescence lifetime and integrated intensity with H_2 is attributed to quenching in the collisional region of the supersonic expansion. By contrast, He is an ineffective quencher and the observed fluorescence lifetime is approximately equal to the radiative lifetime.

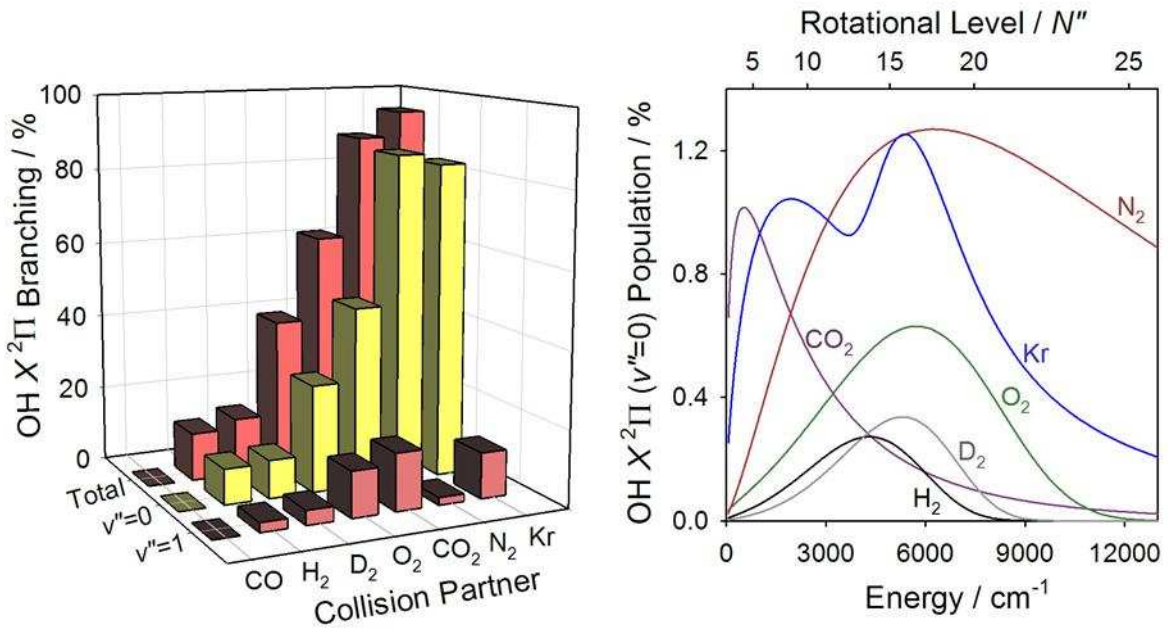

Figure 4. Nonreactive quenching of OH $A\ ^2\Sigma^+$ (v'=0, N'=0) by various collision partners results in OH $X\ ^2\Pi$ (v''=0-2, N'') products. The total branching to OH $X\ ^2\Pi$ (v''=0-2) as well as the separate OH $X\ ^2\Pi$ (v''=0) and (v''=1) components are shown in the left-hand panel. Rotational distributions of OH $X\ ^2\Pi$ (v''=0, N'') products are plotted as a function of rotational energy and rotational level (N'') in the right-hand panel. The distributions are fits to experimental data from Refs. (13-15, 17-19), scaled such that the integrated areas correspond to the branching to OH $X\ ^2\Pi$ (v''=0) for each collision partner.

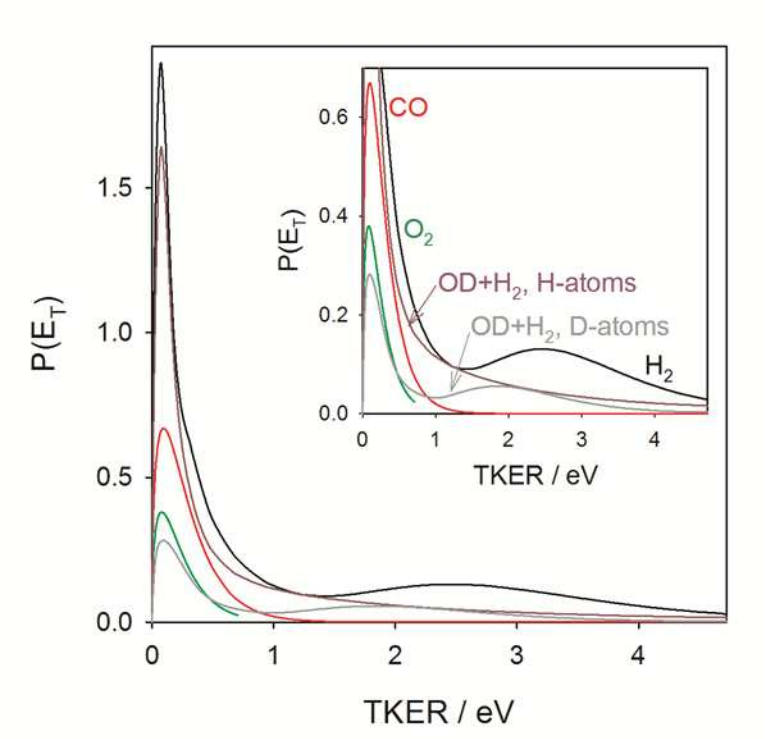

Figure 5. Translational energy distributions $P(E_T)$ as a function of total kinetic energy released (TKER) following reactive quenching of OH/D $A\ ^2\Sigma^+$ (v'=0) by different collision partners. The fits to experimental data from Refs. (20, 23) are scaled such that the integrated area corresponds to the branching to the reactive pathway producing H- or D-atoms for each collision partner. The inset shows a magnification of the ordinate axis.

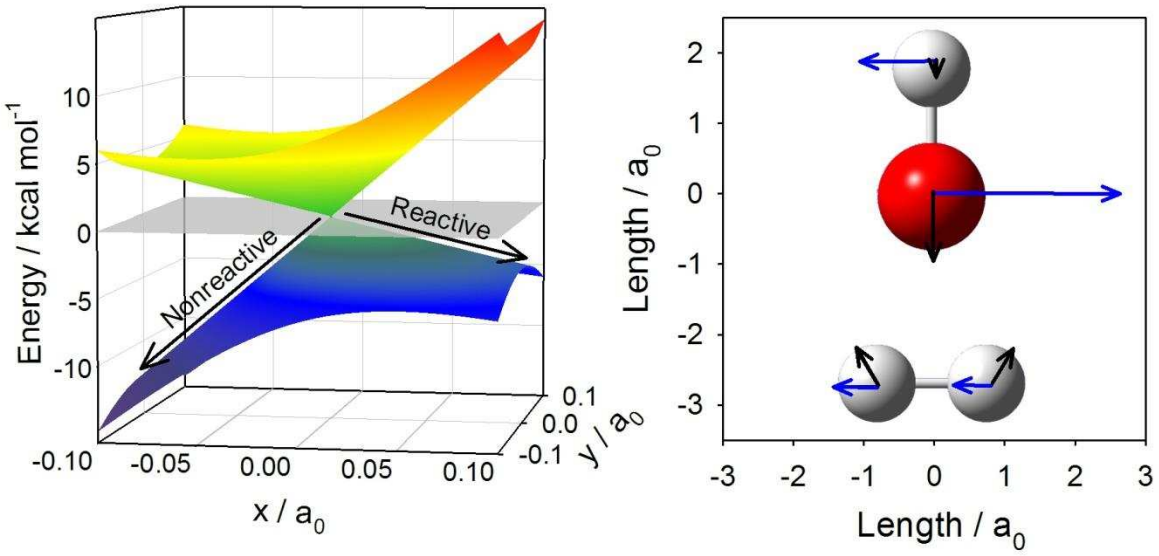

Figure 6. A three dimensional plot of a representative C_{2v} cone of intersection in the OH ($A\,^2\Sigma^+$, $X\,^2\Pi$) + H_2 system (left) and Cartesian representation of the **g** (energy difference, black arrow) and **h** (interstate coupling, blue arrow) vectors (right) adapted from Figure 2a of Ref. (26). The **g** vectors drive the OH and H_2 moieties toward or away from one another as they approach and exit from the CI, ultimately leading to reactive or nonreactive quenching. The **h** vectors illustrate the torque being placed on the OH radical in the vicinity of the CI. The **g** and **h** vectors lie along the x and y coordinates, respectively, and zero energy is defined as the branching plane.

References

1. Glassman I, Yetter R. 2008. *Combustion, Fourth Edition*. Boston: Academic Press
2. Wayne RP. 2000. *Chemistry of Atmospheres, Third Edition*. Oxford: Oxford University Press
3. Luque J, Crosley DR. 1999. LIFBASE: Database and Spectral Simulation Program (Version 1.6). *SRI International Report MP 99-009*
4. Copeland RA, Crosley DR. 1986. Temperature dependent electronic quenching of OH($A\ ^2\Sigma^+$, v'=0) between 230 and 310 K. *J. Chem. Phys.* 84: 3099-105
5. Heard DE, Henderson DA. 2000. Quenching of OH($A^2\Sigma^+$, v' = 0) by Several Collision Partners between 200 and 344 K. Cross-Section Measurements and Model Comparisons. *Phys. Chem. Chem. Phys.* 2: 67-72
6. Retail B, Orr-Ewing AJ. 2010. *Processes Involving Multiple Potential Energy Surfaces*. In *Tutorials in Molecular Reaction Dynamics*, ed. M Brouard, C Vallance. Cambridge: Royal Society of Chemistry
7. Crim FF. 2012. Molecular reaction dynamics across the phases: similarities and differences. *Faraday Discuss.* 157: 9-26
8. Domcke W, Yarkony DR. 2012. Role of Conical Intersections in Molecular Spectroscopy and Photoinduced Chemical Dynamics. *Annu. Rev. Phys. Chem.* 63: 325-52
9. Levine BG, Martinez TJ. 2007. Isomerization through conical intersections. *Annu. Rev. Phys. Chem.* 58: 613-34
10. Matsika S, Krause P. 2011. Nonadiabatic Events and Conical Intersections. *Annu. Rev. Phys. Chem.* 62: 621-43
11. Worth GA, Cederbaum LS. 2004. Beyond Born-Oppenheimer: Molecular dynamics through a conical intersection. *Annu. Rev. Phys. Chem.* 55: 127-58
12. Pollack IB, Lei YX, Stephenson TA, Lester MI. 2006. Electronic quenching of OH $A\ ^2\Sigma^+$ radicals in collisions with molecular hydrogen. *Chem. Phys. Lett.* 421: 324-8
13. Dempsey LP, Murray C, Lester MI. 2007. Product Branching between Reactive and Non-Reactive Pathways in the Collisional Quenching of OH $A^2\Sigma^+$ Radicals by H_2. *J. Chem. Phys.* 127: 151101
14. Dempsey LP, Murray C, Cleary PA, Lester MI. 2008. Electronic Quenching of OH $A^2\Sigma^+$ Radicals in Single Collision Events with H_2 and D_2: A Comprehensive Quantum State Distribution of the OH $X^2\Pi$ Products. *Phys. Chem. Chem. Phys.* 10: 1424-32
15. Dempsey LP, Sechler TD, Murray C, Lester MI. 2009. Quantum State Distribution of the OH $X^2\Pi$ Products from Collisional Quenching of OH $A^2\Sigma^+$ by O_2 and CO_2. *J. Phys. Chem. A* 113: 6851-8
16. Cleary PA, Dempsey LP, Murray C, Lester MI, Kłos J, Alexander MH. 2007. Electronic Quenching of OH $A^2\Sigma^+$ Radicals in Single Collision Events with Molecular Hydrogen: Quantum State Distribution of the OH $X^2\Pi$ Products. *J. Chem. Phys.* 126: 204316
17. Lehman JH, Dempsey LP, Lester MI, Fu B, Kamarchik E, Bowman JM. 2010. Collisional Quenching of OD $A^2\Sigma^+$ by H_2: Experimental and Theoretical studies of the State-Resolved OD $X^2\Pi$ Product Distribution and Branching Fraction. *J. Chem. Phys.* 133: 164307
18. Dempsey LP, Sechler TD, Murray C, Lester MI, Matsika S. 2009. State-Resolved Distribution of OH $X^2\Pi$ Products Arising from Electronic Quenching of OH $A^2\Sigma^+$ by N_2 *J. Chem. Phys.* 130: 104307
19. Lehman JH, Lester MI, Kłos J, Alexander MH, Dagdigian PJ, et al. 2013. Electronic Quenching of OH $A^2\Sigma^+$ Induced by Collisions with Kr Atoms. *J. Phys. Chem. A*: Submitted
20. Lehman JH, Lester MI, Yarkony DR. 2012. Reactive Quenching of OH $A^2\Sigma^+$ by O_2 and CO: Experimental and Nonadiabatic Theoretical Studies of H- and O-Atom Product Channels. *J. Chem. Phys.* 137: 094312

21. Anderson DT, Todd MW, Lester MI. 1999. Reactive quenching of electronically excited OH radicals in collisions with molecular hydrogen. *J. Chem. Phys.* 110: 11117-20
22. Todd MW, Anderson DT, Lester MI. 2001. Reactive quenching of OH $A^2\Sigma^+$ in collisions with molecular deuterium via nonadiabatic passage through a conical intersection. *J. Phys. Chem. A* 105: 10031-6
23. Lehman JH, Bertrand JL, Stephenson TA, Lester MI. 2011. Reactive Quenching of OD $A^2\Sigma^+$ by H_2: Translational Energy Distributions for H- and D-Atom Product Channels. *J. Chem. Phys.* 135: 144303
24. Ortiz-Suárez M, Witinski MF, Davis HF. 2006. Reactive Quenching of OH($A^2\Sigma^+$) by D_2 Studied Using Crossed Molecular Beams. *J. Chem. Phys.* 124: 201106
25. Lester MI, Loomis RA, Schwartz RL, Walch SP. 1997. Electronic quenching of OH $A^2\Sigma^+$ (v' = 0, 1) in complexes with hydrogen and nitrogen. *J. Phys. Chem. A* 101: 9195-206
26. Hoffman BC, Yarkony DR. 2000. The Role of Conical Intersections in the Nonadiabatic Quenching of OH($A^2\Sigma^+$) by Molecular Hydrogen. *J. Chem. Phys.* 113: 10091-9
27. Kamarchik E, Fu BN, Bowman JM. 2010. Communication: Classical Trajectory Study of the Postquenching Dynamics of OH $A^2\Sigma^+$ by H_2 Initiated at Conical Intersections. *J. Chem. Phys.* 132: 091102
28. Fu B, Kamarchik E, Bowman JM. 2010. Quasiclassical Trajectory Study of the Postquenching Dynamics of OH $A^2\Sigma^+$ by H_2/D_2 on a Global Potential Energy Surface. *J. Chem. Phys.* 133: 164306
29. Zhang PY, Lu RF, Chu TS, Han KL. 2010. Quenching of OH($A^2\Sigma^+$) by H_2 through Conical Intersections: Highly Excited Products in Nonreactive Channel. *J. Phys. Chem. A* 114: 6565-8
30. Zhang PY, Lu RF, Chu TS, Han KL. 2010. Nonadiabatic Quantum Reactive Scattering of the OH($A^2\Sigma^+$) + D_2. *J. Chem. Phys.* 133: 174316
31. Collins MA, Godsi O, Liu S, Zhang DH. 2011. An ab initio quasi-diabatic potential energy matrix for OH($^2\Sigma^+$) + H_2. *J. Chem. Phys.* 135: 234307
32. Copeland RA, Dyer MJ, Crosley DR. 1985. Rotational-level-dependent quenching of $A^2\Sigma^+$ hydroxyl and hydroxyl-d. *J. Chem. Phys.* 82: 4022-32
33. Fairchild PW, Smith GP, Crosley DR. 1983. Collisional quenching of $A^2\Sigma^+$ hydroxyl at elevated temperatures. *J. Chem. Phys.* 79: 1795-807
34. Kenner RD, Capetanakis FP, Stuhl F. 1990. Kinetic Isotope Effects in the Electronic Quenching of OD/OH(A $^2\Sigma^+$,v'=0) at 296 +/- 4-K. *J. Phys. Chem.* 94: 2441-6
35. Smith GP, Crosley DR. 1986. Quenching of OH ($A^2\Sigma^+$, v' = 0) by H_2, N_2O, and Hydrocarbons at Elevated-Temperatures. *J. Chem. Phys.* 85: 3896-901
36. Creasey DJ, HalfordMaw PA, Heard DE, Pilling MJ, Whitaker BJ. 1997. Implementation and initial deployment of a field instrument for measurement of OH and HO_2 in the troposphere by laser-induced fluorescence. *J. Chem. Soc.-Faraday Trans.* 93: 2907-13
37. Heal MR, Heard DE, Pilling MJ, Whitaker BJ. 1995. On the Development and Validation of FAGE for Local Measurement of Tropospheric OH and HO_2. *J. Atmos. Sci.* 52: 3428-41
38. Heard DE. 2006. Atmospheric field measurements of the hydroxyl radical using laser-induced fluorescence spectroscopy. *Annu. Rev. Phys. Chem.* 57: 191-216
39. Crosley DR. 1989. Rotational and translation effects in collisions of electronically excited diatomic hydrides. *J. Phys. Chem.* 93: 6273-82
40. Hemming BL, Crosley DR. 2002. Rotational-Level Dependence of OH $A^2\Sigma^+$ Quenching at 242 and 196 K. *J. Phys. Chem. A* 106: 8992-5
41. Hemming BL, Crosley DR, Harrington JE, Sick V. 2001. Collisional Quenching of High Rotational Levels in $A^2\Sigma^+$ OH. *J. Chem. Phys.* 115: 3099-104

42. Settersten TB, Patterson BD, Kronemayer H, Sick V, Schulz C, Daily JW. 2006. Branching ratios for quenching of nitric oxide A $^2\Sigma^+$(v '=0) to X $^2\Pi$(v ''=0). *Phys. Chem. Chem. Phys.* 8: 5328-38
43. Zare RN, Herschbach DR. 1963. Doppler Line Shape of Atomic Fluorescence Excited by Molecular Photodissociation. *Proceedings of the IEEE* 51: 173
44. Hancock G, Saunders M. 2008. Vibrational distribution in NO($X^2\Pi$) formed by self quenching of NO A $^2\Sigma^+$ (v = 0). *Phys. Chem. Chem. Phys.* 10: 2014-9
45. Paci MAB, Few J, Gowrie S, Hancock G. Products of the quenching of NO A $^2\Sigma^+$(v=0) by N_2O and CO_2. *Phys. Chem. Chem. Phys.* 15: 2554-64
46. Estupiñán EG, Stickel RE, Wine PH. 2001. An investigation of N_2O production from quenching of OH(A $^2\Sigma^+$) by N_2. *Chem. Phys. Lett.* 336: 109-17
47. von Neumann J, Wigner E. 1929. Uber das Verhalten von Eigenwerten bei adiabatischen Prozessen. *Physikalische Zeitschrift* 30: 467
48. Koppel H, Domcke W, Cederbaum LS. 1984. Multimode Molecular-Dynamics Beyond the Born-Oppenheimer Approximation. *Adv. Chem. Phys.* 57: 59-246
49. Manaa MR, Yarkony DR. 1994. On the Role of Conical Intersections of 2 Potential-Energy Surfaces of the Same Symmetry in Photodissociation. 2. CH_3SCH_3 -> CH_3S+CH_3. *J. Am. Chem. Soc.* 116: 11444-8
50. Yarkony DR. 2001. Nuclear dynamics near conical intersections in the adiabatic representation: I. The effects of local topography on interstate transitions. *J. Chem. Phys.* 114: 2601
51. Yarkony DR. 1998. Conical intersections: Diabolical and often misunderstood. *Acc. Chem. Res.* 31: 511-8
52. Hernandez R, Clary DC. 1995. Electronic-Spectra of the OH ($A^2\Sigma^+$)-H_2 and OH($A^2\Sigma^+$)-D_2 Complexes. *Chem. Phys. Lett.* 244: 421-6
53. Miller SM, Clary DC, Kliesch A, Werner HJ. 1994. Rotationally Inelastic and Bound State Dynamics of H_2-OH($X^2\Pi$). *Mol. Phys.* 83: 405-28
54. Loomis RA, Lester MI. 1995. Stabilization of Reactants in a Weakly-Bound Complex - OH-H_2 and OH-D_2. *J. Chem. Phys.* 103: 4371-4
55. Loomis RA, Lester MI. 1997. OH-H_2 entrance channel complexes. *Annu. Rev. Phys. Chem.* 48: 643-73
56. Loomis RA, Schwartz RL, Lester MI. 1996. Electronic spectroscopy and quenching dynamics of OH-H_2/D_2 pre-reactive complexes. *J. Chem. Phys.* 104: 6984-96
57. Yarkony DR. 1996. Current Issues in Nonadiabatic Chemistry. *J. Phys. Chem.* 100: 18612-28
58. Yarkony DR. 1999. Substituent Effects and the Noncrossing Rule: The Importance of Reduced Symmetry Subspaces. I. The Quenching of OH($A^2\Sigma^+$) by H_2. *J. Chem. Phys.* 111: 6661-4
59. Vegiri A, Farantos SC. 1988. *Electronic Deexcitation of OH(A $^2\Sigma^+$) with CO(X $^1\Sigma^+$): An ab initio Study*. In *Selectivity in Chemical Reactions*, ed. JC Whitehead, pp. 393-402: Kluwer Academic Publishers
60. Vegiri A, Farantos SC. 1990. A Classical Dynamical Investigation of the Mechanism of Electronic Quenching of OH(A $^2\Sigma^+$) in Collisions with CO(X $^1\Sigma^+$). *Mol. Phys.* 69: 129-46
61. Bearpark MJ, Robb MA, Schlegel HB. 1994. A Direct Method for the Location of the Lowest Energy Point on a Potential Surface Crossing. *Chem. Phys. Lett.* 223: 269-74
62. See the Supplemental Material link in the online version of this article or http://www.annualreviews.org/. Reprinted with permission from Lehman JH, Dempsey LP, Lester MI, Fu B, Kamarchik E, Bowman JM. 2010. *J. Chem. Phys.* 133: 164307, Copyright 2010, American Institute of Physics.
63. Hancock G. 2013. personal communication.

64. Conte R, Fu B, Kamarchik E, Bowman JM. 2013. A novel Gaussian Binning (1GB) analysis of vibrational state distributions in highly excited H_2O from reactive quenching of OH* by H_2. *J. Chem. Phys.*: Accepted
65. Truhlar DG, Bowman JM. 2013. Personal Communication.
66. Dillon J, Yarkony DR. 2013. On the Mechanism for the Nonadiabatic Reactive Quenching of OH ($A\ ^2\Sigma^+$) by H_2 ($^1\Sigma_g^+$). The Role of the $2\ ^2A$ State. *J. Chem. Phys.*: Accepted